Model-Independent Analysis of Pyrene Photokinetics in SDS Micelles

Michele M. Villegas[†] and Sharon L. Neal*

Department of Chemistry, University of California at Riverside, Riverside, California 92521

Received: January 10, 1997; In Final Form: April 19, 1997[⊗]

In this report, the dependence of pyrene photokinetics on sodium dodecyl sulfate (SDS) micelle concentration is investigated *via* dynamic multidimensional fluorescence measurements. First, complex quantum yield matrices were constructed from steady-state spectra and multiple wavelength phase/modulation data. These matrices were then subjected to rank analysis in order to determine the number of spectrally distinct pyrene components. The consensus of these results is that there are three spectrally distinguishable pyrene components. Then, the emission spectra of the pyrene components, their relative initial concentrations, and the photokinetic transfer matrix, which describes their decay and interaction, are estimated without model assumptions. The characteristics of the fluorescence spectra and their dependence on the SDS concentration identify the three components as pyrene excimer, aggregates, and monomers. The results also indicate that pyrene decay kinetics in SDS micelles vary substantially with the SDS concentration. At low surfactant concentration, pyrene decays *via* an irreversible 3-state mechanism. As the surfactant concentration is increased, the rate of the rate of the excimer dissociation reaction increases and the mechanism becomes reversible.

Introduction

Pyrene is one of the most widely used probes of microheterogeneous media because of the flexibility provided by its unique combination of spectral and kinetic properties. The vibronic band intensities of the monomer spectrum exhibit a dependence on the solvent polarity.[1] Consequently, the ratio of monomer emission bands I ($\lambda \sim 373$ nm) and III ($\lambda \sim 384$ nm) have been used to determine the local polarity of many media.[2,3] Excited pyrene monomers also form excimers in concentrated solution. The excimer spectrum is substantially red-shifted relative to the monomer spectrum, and the ratio of monomer emission bands ($\lambda \sim 400$ nm) to excimer emission bands ($\lambda \sim 470$ nm) has been used as an indicator of concentration dependent medium properties.[4−6] Pyrene has a very long intrinsic fluorescence lifetime which leads to a decay rate that is particularly sensitive to the local environment of the probe. The lifetime of pyrene in oxygen-free SDS micelles is greater than 300 ns, but less than 200 ns in premicellar SDS solutions.[2] Consequently, the lifetime is a prime indicator of pyrene inclusion in hydrophobic media. Pyrene excimer decay kinetics also are used to characterize structural features and concentration dependent phenomena in organized media. Excimer formation rates have been linked to membrane "fluidity" and localized differences in probe distribution in microheterogeneous media.[7]

This brief overview of the role of pyrene excimer kinetics in medium characterization belies the complexity of pyrene photokinetics in microheterogeneous media and the difficulty of excimer decay analysis. The analysis of excimer photokinetics was pioneered by Birks who described the time evolution of pyrene monomers and excimers using a pair of coupled linear differential equations.[8] In this model, only the pyrene monomer is radiatively excited; the excimer is formed *via* a diffusion-controlled reaction between a ground-state and excited monomer. The dimer complex is dissociative in the ground state and therefore only observed in the excited state. This "two-state" model successfully described pyrene excimer formation in isotropic solvents. Consequently, it was used as the basis of studies correlating the excimer formation rate, or its corollary, the excimer/monomer intensity ratio, to concentration dependent phenomena in membranes.[4,9] However, observations in several media have been reported in the literature that are inconsistent with the original two-state model. Pyrene excimer emission with no apparent rise time, implying the presence of ground-state aggregates, has been measured by time-resolved spectroscopy in pyrene-labeled polymers.[10] Excimer emission has been observed from dilute solutions of water-soluble pyrene derivatives in surfactant solutions below the surfactant critical micelle concentration (cmc).[11] Theoretical calculations also support the existence of ground-state aggregates in pyrene crystals.[12] Attempts to apply the two-state model to the emission of pyrene solubilized in anisotropic media have not been successful.[13−15] Most importantly, Blackwell *et al.* demonstrated that the dependence of excimer emission on pyrene concentration is not consistent with diffusion-controlled excimer formation in several lipid membranes.[16]

The debate about the generality of the two-state model has faded, but questions remain concerning the details of excimer kinetics in various media. Influenced by the observations of Blackwell *et al.*, several studies have been based on three-state models, which include self-quenched pyrene monomers, to analyze excimer emission.[7,17,18] However, the addition of this third component does not resolve all questions concerning the excimer formation mechanism. Figure 1 depicts two three-state models that have been used to analyze excimer emission in membranes and the kinetic transfer matrices which describe them. Theoretically, there are more than 30 possible models that might be observed in the case of three-state excimer formation. Selecting one of these models and negotiating the difficulties which arise from the increase in the number of required fitting parameters are not trivial tasks. When the inherent ambiguity of model selection and the skepticism which should meet all analyses based on three or more exponentials[19] are considered, the reliability of nonlinear least-squares analysis based on three-state models is debatable.

Recently, it has been demonstrated that it is possible to analyze wavelength-dependent frequency-domain fluorescence data without model assumptions when the underlying photokinetic mechanism is described by a system of coupled first-order

[†] Present address: Allergan, Inc., 2525 Dupont Dr., P. O. Box 19534, Irvine, CA 92713-9534.

[⊗] Abstract published in *Advance ACS Abstracts,* June 1, 1997.

S1089-5639(97)00171-0 CCC: $14.00

differential equations with constant coefficients.[20] Emission-frequency-domain decay matrices comprised of complex quantum yields[21] measured over a range of emission wavelengths and excitation modulation frequencies can be partitioned into spectral and kinetic factors from which the species associated emission spectra[22] of the sample components, their initial excited state intensities, and the photokinetic matrix describing excited state interactions can be determined. Statistical methods can be used to estimate the number of emitting components, so that every aspect of the analysis can be pursued without *a priori* assumptions. Moreover, the simultaneous estimation of the component spectra and initial concentrations associated with the decaying components is useful in establishing the validity of the mechanism indicated by the transfer matrix when more than two fluorophores are involved. The method is completely general: it has also been applied to the decay analysis of fluorophore mixtures in which excited state reactions do not occcur.[23]

In this report, the matrix-formatted wavelength-dependent frequency-domain fluorescence of pyrene in sodium dodecyl sulfate (SDS) solution, above but close to the cmc, is subjected to model-independent frequency-domain analysis. SDS is considered the prototype anionic surfactant by many researchers and thus has been the focus of exhaustive study.[24] Typically, a low, and therefore homogeneously solubilized, pyrene concentration is used in probe studies, but excimer formation studies usually require higher local pyrene concentrations and are thus facilitated by SDS concentrations which are closer to the cmc. Lifetimes[25] and spectral changes observed in pyrene spectra during Cu^{2+} quenching studies[26] indicate that the pyrene monomer has at least two spectrally and temporally distinct components when solubilized in SDS solutions whose concentrations are close to the cmc. The goal of the work reported here is to discover the mechanistic details of pyrene excimer kinetics in SDS from the spectra, initial concentrations, and photokinetic transfer matrices associated with pyrene emission and their dependence on the SDS concentration.

The following notation is used throughout this paper. Matrices are denoted by uppercase, boldface Roman and Greek letters, and vectors are denoted by lowercase, boldface Roman and Greek letters. Scalars are denoted by lowercase, italic Roman and Greek letters. Complex variables are indicated using a superpositioned tilde (*i.e.*, $\tilde{\mathbf{M}}$). As usual, superscript^{-1} denotes the matrix inverse, and the slanted prime ($'$) denotes the matrix transpose.

Materials and Methods

Materials. In the experiments described here, the following reagents were used as received: sodium dodecyl sulfate (99% purity, Sigma Chemical Co.), pyrene (99% purity, Aldrich Chemical Co.), *p*-bis(2-(5-phenyloxzoyl))benzene (POPOP) (Exciton Chemical Co., Inc.). Methylene Chloride (Fisher or Burdick and Jackson) and ethyl alcohol (absolute, 200 proof, Quantum Chemical Co.) were purchased at the highest available purity. All aqueous solutions were prepared using doubly distilled−deionized water.

Freshly prepared SDS solutions were used for all measurements. The pyrene in SDS solutions were prepared by coating a stock solution of pyrene in methylene chloride onto the sides of a round bottom flask and placing it under high vacuum at approximately 50 °C overnight (at least 10 h). SDS was then weighed into the flask and diluted with water to the appropriate concentration. The samples were sonicated in a bath sonicator for approximately 30 min, cooled to room temperature, and then purged with Argon for more than 1 h prior to data acquisition. The cmc of SDS is reportedly 8.2 mM.[27] Emission-frequency-domain decay matrices were acquired using solutions which contained 6.85×10^{-5} M pyrene in 9, 11, 16, and 33 mM SDS, respectively. Replicate measurements of each matrix were acquired. The micelle concentration was calculated using a value of 60 for the aggregation number and 7.5 mM as the concentration of free monomer in solutions above the cmc.[27] The concentration of micelles in these solutions was calculated using the expression

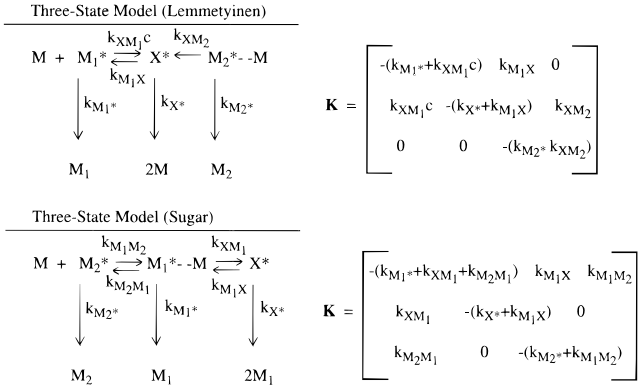

Figure 1. Two of the three-state models that have been used to analyze excimer emission in membranes and their corresponding kinetic transfer matrices. See references 17 and 18.

$$[\text{micelle}] = \frac{[\text{SDS}]_{\text{total}} - [\text{SDS}]_{\text{monomer}}}{N_{\text{agg}}} \qquad (1)$$

The concentration of micelles calculated for these solution are 0.024, 0.058, 0.142, and 0.425 M.

Fluorescence Measurements. Fluorescence lifetime measurements were acquired using a multifrequency cross-correlation phase-modulation spectrofluorometer (K2, ISS, Champaign, IL). Excitation at 351 nm was provided by a 5W argon ion laser (Innova-90, Coherent, Santa Clara,CA). The fluorescence emission was collected at 90° to the excitation, dispersed by a spectrograph equipped with a 150 groove/mm grating (HR320, Instruments SA, Metuchen, NJ) and monitored using a 1024 element microchannel plate intensified photodiode array detector (IRY-1024 , Princeton Instruments, Trenton, NJ). For each measurement, the excitation beam was sinusoidally modulated at 10 to 18 logarithmically spaced frequencies between 0.3 and 15 MHz. The lifetime data was acquired using POPOP in ethanol as the reference lifetime standard. The reference lifetime was assigned the widely accepted value of 1.35 ns.[28] At each modulation frequency, the fluorescence emission at each diode was converted to modulation, phase, and steady-state intensity values and stored.

Data Analysis

All data analysis was performed on a SPARC 20 Unix workstation (Sun Microsystems, Palo Alto, CA) and using software written by the author in MATLAB, an interactive programming language for matrix operations with graphics (The Mathworks, Natick, MA). Experimental phase data was corrected for (n180°) phase flips and filtered using a second-order Butterworth low-pass filter. Phase and modulation data acquired on approximately 200 pixels (370 and 475 nm) at up to 18 modulation frequencies between 0.3 and 15 MHz were combined to form a single complex data matrix.

Matrix Construction. The emission-frequency-domain decay matrix is comprised of the complex quantum yield measured at a number of emission wavelengths and excitation modulation frequencies. The elements of the matrix are calculated from the experimental steady-state spectrum, phase shift, and modula-

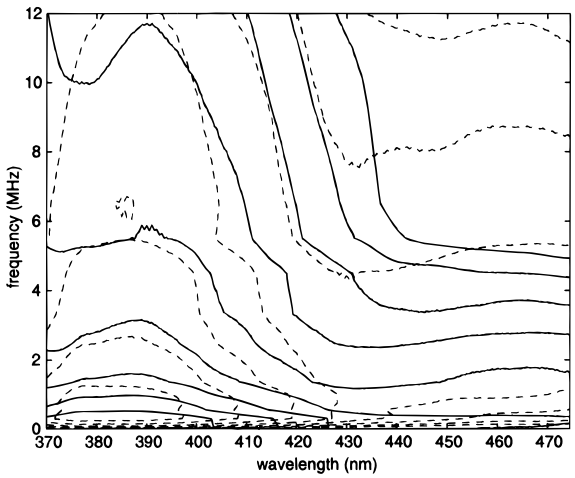

Figure 2. Contour plot of the emission-frequency domain decay matrix of pyrene solubilized in 16 mM SDS: solid lines, real values; dashed lines, complex values.

tion factor:

$$\tilde{d}(\lambda,\omega) = s(\lambda,0)m(\lambda,\omega)e^{i\phi(\lambda,\omega)} \quad (2)$$

where $d(\lambda,\omega)$ is the λth, ωth element of the emission-frequency-domain decay matrix $\tilde{\mathbf{D}}$, $s(\lambda,0)$ is a scalar representing the intensity of the steady-state spectrum of the sample at wavelength λ, $m(\lambda,\omega)$ is the modulation factor, and $\phi(\lambda,\omega)$ is the phase shift at wavelength and modulation frequency ω. A contour plot of the emission-frequency domain decay matrix of pyrene solubilized in 16 mM SDS is shown in Figure 2.

Pseudorank Estimation. The first step in the analysis of all matrix-formatted fluorescence data is the determination of the number of fluorophores giving rise to the observed data. Ideally, the rank of a fluorescence data matrix is equal to the number of fluorophores which emit distinct spectra. In practice, the rank of experimental matrices is greater than the number of fluorophores, due to the superimposition of measurement errors on the fluorescence signal. A number of "pseudorank" estimation methods have been developed to estimate the number of signal components in the presence of noise components. These methods are described in detail elsewhere.[29−31]

Since the emission-frequency-domain decay matrix $\tilde{\mathbf{D}}$ is complex, an alternative approach to pseudorank estimation which capitalizes on the data structure was developed for the data analyzed in this investigation. The matrix $\tilde{\mathbf{D}}$ is the product of the emission spectra and the frequency-domain decays of the components. While the spectra and decays are not known prior to the analysis, the matrix can always be partitioned into the product of two orthogonal matrices which are linear combinations of the fluorescence spectra and frequency-domain decays, respectively. Mathematically, these relationships are stated

$$\tilde{\mathbf{D}} = \tilde{\mathbf{U}}\,\tilde{\mathbf{Q}}' = \mathbf{X}\,\tilde{\mathbf{Y}}' \quad (3)$$

where the digitized emission spectra of the components are stored along the columns of $\mathbf{X}$, and the digitized frequency-domain decays of the components are stored along the columns of $\tilde{\mathbf{Y}}$. $\tilde{\mathbf{U}}$ and $\tilde{\mathbf{Q}}'$ are orthogonal ($\tilde{\mathbf{U}}$ is orthonormal) basis vectors which span the same vector spaces as $\mathbf{X}$ and $\tilde{\mathbf{Y}}$. The number of basis vectors (*i.e.*, columns of $\tilde{\mathbf{U}}$ and $\tilde{\mathbf{Q}}'$ required to reconstruct $\tilde{\mathbf{D}}$ is the rank) the number required to reconstruct the spectral signal embedded in $\tilde{\mathbf{D}}$ with as little noise as possible is the pseudorank n. It is evident from equation 3 that $\tilde{\mathbf{U}}$, which is complex, is comprised of linear combinations of the spectra, $\mathbf{X}$. In fact, both the real and imaginary parts of $\tilde{\mathbf{U}}$ are linear combinations of $\mathbf{X}$. The pseudorank of $\tilde{\mathbf{D}}$ can be estimated by

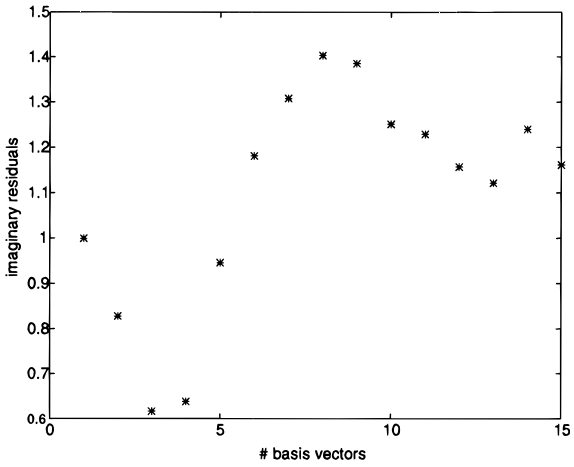

Figure 3. Pseudorank estimation of the emission-frequency-domain decay matrix of pyrene solubilized in 16 mM SDS. The points are the sum of the squared residuals of the imaginary basis divided by the squared number of components. The minimum residual indicates the optimal number of components.

measuring the capacity of the real part of $\tilde{\mathbf{U}}$ to form a basis for the imaginary part of $\tilde{\mathbf{U}}$. If one attempts to describe the imaginary components of $\tilde{\mathbf{U}}$ as combinations of fewer than the first n basis vectors constructed from the real components of $\tilde{\mathbf{U}}$, there will be a significant difference between the original and projected imaginary components. Large residuals will be observed indicating that the real basis vectors were inadequate to describe the imaginary components. If the imaginary components of $\tilde{\mathbf{U}}$ are described as combinations of n or more real components of $\tilde{\mathbf{U}}$, the size of the residuals will be essentially the same. The imaginary components of $\tilde{\mathbf{U}}$ not described by a combination of the first k real components of $\tilde{\mathbf{U}}$ (*i.e.,* the residuals after projection onto the vector space constructed from the real part of the first k columns of $\tilde{\mathbf{U}}$) are given by the expression

$$(\tilde{\mathbf{U}}^{\text{imag}}_{\text{res}})_k = (\mathbf{I} - \tilde{\mathbf{U}}^{\text{real}}_{1:k}\tilde{\mathbf{U}}^{\text{real}\prime}_{1:k})\tilde{\mathbf{U}}^{\text{imag}} \quad (4)$$

where $\mathbf{I}$ is the $r \times r$ identity matrix and $\tilde{\mathbf{U}}^{\text{real}}_{lk}$ indicates the first k columns of the real part of $\tilde{\mathbf{U}}$. The sum of the squared residuals of the imaginary basis calculated from the emission-frequency domain decay matrix acquired from pyrene in 16 mM SDS solution is illustrated in Figure 3. The size of the residuals indicate that the pseudorank of the matrix is 3.

Emission Frequency Domain Decay Matrix Partitioning. In this study, the spectra of the emitting components are not known because the spectra depend on the local environment of the probe. In order to perform a model-independent photokinetic analysis, the emission-frequency-domain decay matrix must be partitioned into spectral and kinetic factors. In other words, the orthogonal basis vectors $\tilde{\mathbf{U}}$ and $\tilde{\mathbf{Q}}$ must be transformed into the component spectra and frequency-domain decays $\mathbf{X}$ and $\tilde{\mathbf{Y}}$. The initial concentrations and photokinetic matrix, $\mathbf{Y}_0$ and $\mathbf{K}$, are then calculated from $\tilde{\mathbf{Y}}$. This transformation can be carried out by minimizing the length of a vector-valued objective function whose elements record the deviation of the spectral and kinetic estimates from the mathematical constraints imposed by nature on spectra, concentrations, and transfer matrix elements. In the analyses reported here the negative and imaginary components of $\mathbf{X}$, the negative and imaginary components of $\mathbf{Y}_0$, the positive diagonals of $\mathbf{K}$, the negative off-diagonals of $\mathbf{K}$, the off-diagonal sums of $\mathbf{K}$, which are larger than the corresponding diagonal elements, the χ^2 between the experimental and reconstructed matrices, and the deviations of the lengths of the spectra from their quantum yield

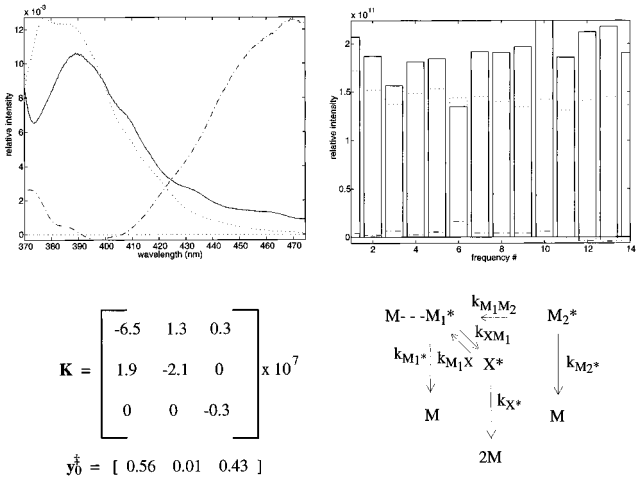

Figure 4. Factors estimated from the emission-frequency domain decay matrix of pyrene solubilized in 16 mM SDS. (4a) Spectra of the pyrene components. (4b) The initial concentrations of the three components as measured at the various modulation frequencies. (4c) The photokinetics transfer matrix, relative initial concentrations, and the associated kinetic mechanism. Negative off-diagonal transfer matrix elements have been replaced by zero. See text for further discussion.

values were used to construct the objective function vector. The χ^2 function measures the agreement between the experimental data matrix, $\tilde{\mathbf{D}}$, and matrices reconstructed from idealized spectra and decays from which inconsistent elements have been deleted $\tilde{\mathbf{D}}$. The reconstructed matrix can be computed using idealized matrices as follows,

$$\tilde{\mathbf{D}}^* = \mathbf{X}^*(\mathrm{K}^*)^{-1}(\tilde{\mathbf{Y}} - \mathbf{Y}_0^*) \tag{5}$$

where the asterisk superscript indicates deletion of inconsistent values from the matrix. The χ^2 function which measures this agreement is given by the expression

$$\chi^2 = \frac{1}{\nu_{\tilde{\mathbf{D}}}} \sum_{\lambda,\omega} \left(\frac{\tilde{\mathbf{D}}^* - \tilde{\mathbf{D}}}{\sigma_{\tilde{\mathbf{D}}}} \right)^2 \tag{6}$$

The values of $\sigma_{\tilde{\mathbf{D}}}$ (an $r \times c$ matrix) were determined from the standard deviations of the steady-state intensity σ_s, modulation σ_m, and phase shift σ_ϕ, using the variance derived from eq 2 by error propagation. The values of σ_s, σ_m, and σ_ϕ varied between 3% and 5% of the steady-state intensity, 0.0075 and 0.015, and 0.026 and 0.044 radians, respectively. The partitioning routine was initialized using the most dissimilar positive, real spectra which could be constructed from the orthogonal basis vectors.[32] Further details of this transformation are given elsewhere.[20]

Results and Discussion

The number of fluorescent components in the pyrene/SDS solutions was determined using the pseudorank estimation procedure described above. In all eight cases, two replicates of four solutions, the number of components was determined to equal three. The factors resolved from a representative emission-frequency-domain decay matrix, pyrene solubilized in 16 mM SDS, are depicted in Figure 4. In Figure 4a, the three spectra which are typical of the spectra estimated from the pyrene solutions at all four SDS concentrations, are shown. There are two spectra whose wavelength ranges identify them as monomer spectra; the third is clearly the excimer spectrum as it is substantially red-shifted. In this work, the quantum yeilds of the three components were each assigned a value equal to 1. Sugar *et al.* found that the ratio of monomer and excimer quantum yields was nearly equal to 1, (*i.e.*, 0.94 ± 0.19 using a 3-state model similar to the one recovered here in a study of

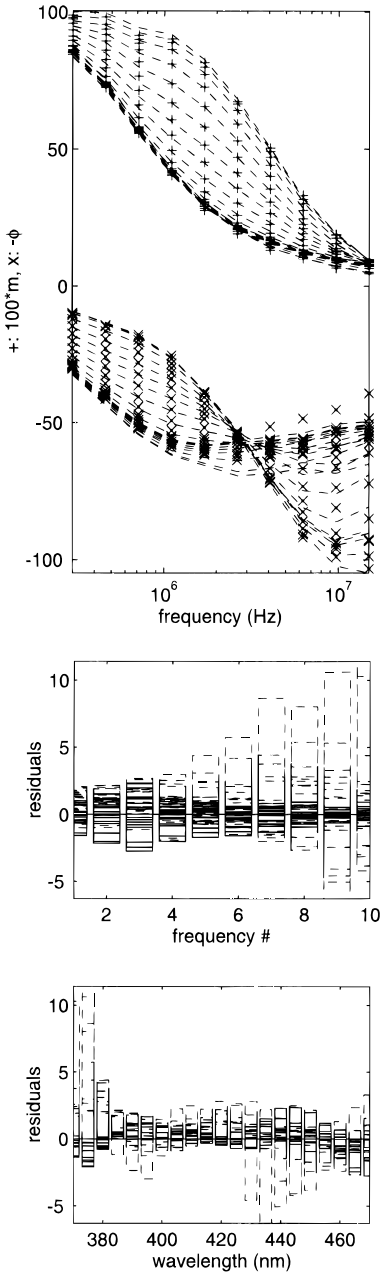

Figure 5. The agreement between the experimental data and data simulated from the analysis results. (5a) Experimental and theoretical modulation and negative phase values. (5b) Residuals as a function of modulation frequency. (5c) Residuals as a function of wavelength.

pyrene-labeled lipids.[18] The suitability of these values is reflected in the agreement between the excimer formation rates reported here and those reported elsewhere in the literature. (See discussion below.) In Figure 4b, the initial concentrations of the three components as measured at the various modulation frequencies are shown. The standard deviation in these values reflects both the data quality and the validity of the spectra and photokinetic matrix. The concentration estimates of the short-lived component exhibits the greatest degree of variation indicating that it is the component most effected by measurement error as would be expected in a frequency-domain measurement. The average relative initial concentrations are 0.56, 0.01, and 0.43. In Figure 4c, the photokinetics transfer matrix and the associated kinetic mechanism are depicted. The photokinetic transfer matrix indicates that the decay times observed from this system are 14, 63, and 333 ns, respectively. Figure 5 illustrates the agreement between the experimental data and data simulated from the analysis results. The agreement is comparable across the wavelengths and frequencies. The deviations

TABLE 1: χ^2-squared Values for Data Sets Analyzed

	data set 1	data set 2
9 mM SDS	2.1	0.9
11 mM SDS	1.1	3.5
16 mM SDS	1.8	0.8
33 mM SDS	16.1	6.3

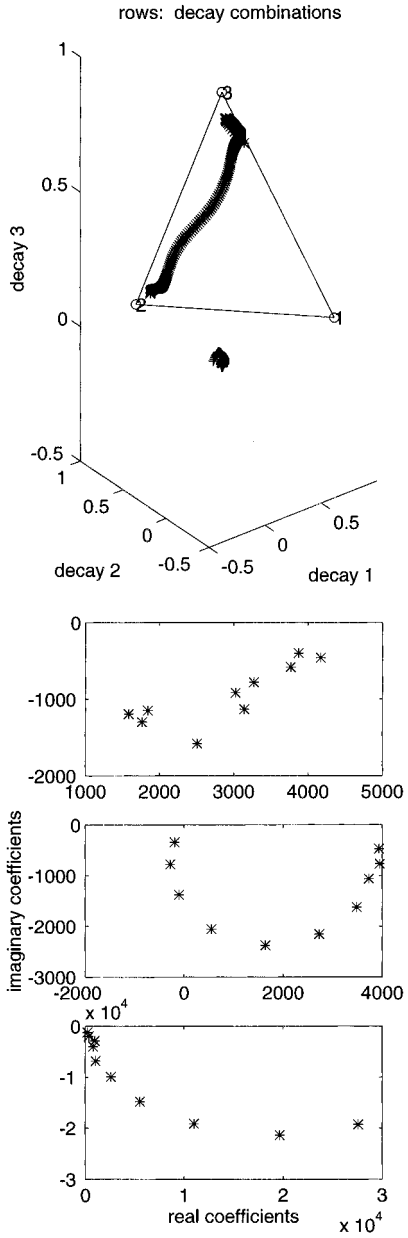

Figure 6. (6a) Scatter plots of the row coordinates of the emission-frequency-domain decay matrix of pyrene solubilized in 16 mM SDS. (6b) Argand plots of the column coordinates of pyrene solubilized in 16 mM SDS.

are highest, as expected, at high frequencies and wavelengths at which the steady-state intensity is low. The average χ^2 values measuring the agreement between the experimental and constructed data matrices for the eight matrices analyzed for this report are listed in Table 1. These results indicate that although the decays in 33 mM SDS exhibit higher residuals than the rest; there is good overall agreement between the experimental and simulated results at the SDS concentrations used in this study.

The results of the graphical analysis of the factors, attributed to pyrene solubilized in 16 mM SDS, are depicted in Figure 6. The scatter plot of the matrix row coordinates indicates that the excimer spectrum has the expected characteristic base line: there are row coordinates near the vertex of the simplex defined

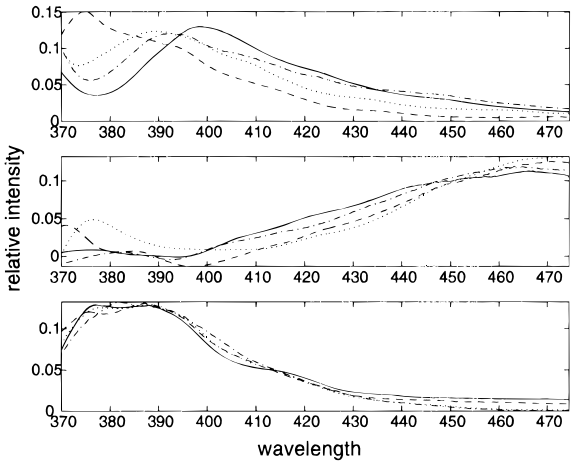

Figure 7. The dependence of the three types of pyrene spectra on the concentration of SDS. (7a) Short-lived monomer spectra. (7b) Excimer spectra. (7c) Long-lived monomer spectra: solid lines, 4 mM SDS; dot−dashed lines, 11 mM SDS, dotted lines, 16 mM SDS; dashed lines, 33 mM SDS.

by the excimer spectrum and there are coordinates on the edge connecting the coordinates of the monomer spectra. The Argand plots of the excimer and long-lived components have shapes that are consistent with a three-state system including a collisionally excited excimer.

The dependence of the three types of pyrene spectra on the concentration of SDS is illustrated in Figure 7. The distortion in the emission spectra and extremely short lifetimes associated with the first spectrum are consistent with the interpretation that the corresponding pyrene molecules are quenched by self-association. The concentration dependence of the spectral distortion corroborates this idea. The spectrum of this component in the 33 mM SDS solution shows no distortion and, unlike the spectra of the third component, is consistent with the spectrum of pyrene solubilized in hydrophilic environments. The emission resolution is insufficient to measure the vibronic band ratios of these monomer spectra,[1] but there is clear difference in the shape of the spectrum emitted by the short-lived and long-lived pyrene molecules. Moreover, that difference is consistent with the conclusion that the short-lived spectrum is emitted by molecules experiencing a more hydrophilic environment, while the long-lived spectrum is emitted by molecules experiencing a more hydrophobic environment. In fact, the long decay time is in itself an indication that these pyrene molecules are sequestered by the surfactant micelles. Changes in the profile of the long-lived spectrum are very small and do not effect the overall shape. Interestingly, there is also a small red-shift and a small band near 370 nm in the excimer spectrum as the SDS concentration increases.

The dependence of the relative initial concentrations of the excited state components on the SDS concentration is depicted in Figure 8. As expected, as the concentration of micelles increases, the sequestered monomer component grows and the self-quenched monomer concentration falls. Interestingly, although it has been definitively demonstrated that probe distribution in surfactant micelles generally is described by Poisson statistics,[33] the intensities of the relative concentration of the self-quenched monomer component does not fall as quickly as the predicted probability of multiple micelle occupancy. This result supports the hypothesis that a significant fraction of the pyrene monomer has formed aggregates and is consistent with an earlier study of pyrene in distearyldimethylammonium bilayer disks in which a nonrandom monomer distribution was observed.[7] However, these results also are consistent with an increase in the quantum yield of the self-quenched monomer as the SDS concentration is increased. The

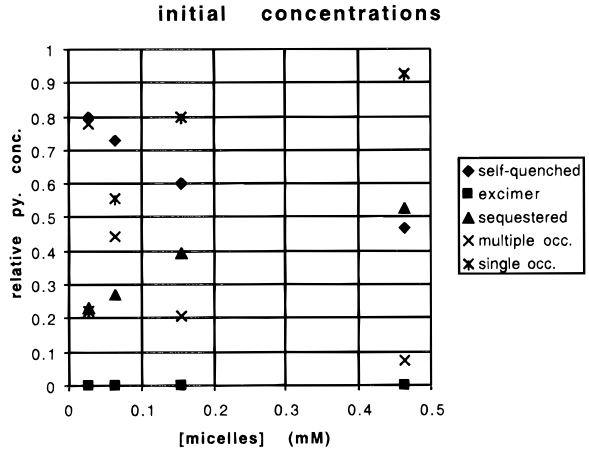

Figure 8. The dependence of the relative initial concentrations of the excited state components on the SDS concentration.

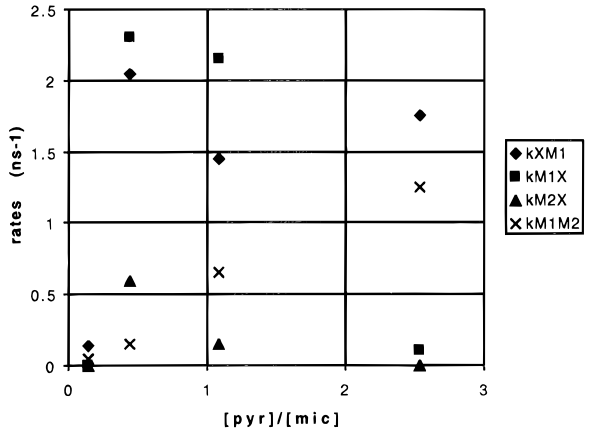

Figure 9. The dependence of the monomer self-association and excimer formation and dissociation rates on the SDS concentration.

initial concentration of the excimer component is expected to equal zero if the excimer is collisionally, as opposed to radiatively excited. In our preliminary analyses, the excimer fractional concentration was not fixed, but we found that setting this value to zero eliminated convergence difficulties as evidenced by terminal objective function values and the number of iterations to convergence. This step also improved indications of the quality of the results, namely the χ^2 values and the standard deviation of the initial concentrations associated with the various modulation frequencies.

The average photokinetic rates estimated from the pyrene fluorescence data at all four SDS concentrations are listed in Table 2. Rates corresponding to negative off-diagonal matrix elements are set to zero in Table 2. (This practice is useful in the calculation of simulated data for χ^2 calculations. If all the matrix components were used without change, the χ^2 estimates would always equal zero.) The only process observed at all four SDS concentrations is the formation of excimers from the shorter-lived monomers. Interestingly, excimer formation from the long-lived monomer and aggregate dissociation to long-lived monomer are never observed. The concentration dependence of the monomer self-association, excimer formation, and excimer dissociation rates is depicted in Figure 9. In this graph, the SDS concentration has been converted to a ratio of pyrene to micelle concentrations to emphasize correlations to the average micelle occupancy number. The monomer self-association rate k_{M1M2} increases, as expected, with the average micelle occupancy. In fact, the dependence is linear. Interestingly, the rate values are larger than the absolute values of the sequestered monomer, decay rates k_{M2}, in 9 and 11 mM SDS. Both sets of values cannot be accurate; the sequestered monomer would have a rate of fluorescence below zero. The k_{M1M2} values are not inflated by inaccurate quantum yields either. The probability that the self-quenched monomer has a higher quantum yield than the sequestered monomer must be close to zero. Since the rates are 1−2 orders of magnitude smaller than the decay rates, we suspect that the inflation of these transfer matrix values can be attributed to numerical limitations.

The rates in Table 2 also indicate that the excimer formation mechanism changes with the SDS concentration. In the 9 and 33 mM SDS solutions, the excimer formation mechanism is irreversible, (*i.e.*, the excimer dissociation rates, k_{M1X} and k_{M2X}, observed are negligible). In the case of the 33 mM SDS solution, the excimer formation rate k_{XM1} is also low; therefore, it is likely that the excimer dissociation rates are too small to be measured under the conditions used in this report. The situation is quite different in the 9 mM SDS solution, the excimer formation rate is high yet very little dissociation is observed. In the 11 and 16 mM solutions, reversible excimer formation kinetics are observed. In fact, the rates of excimer dissociation to self-quenched k_{M1X} and sequestered monomers k_{M2X} both increase as the average micelle occupancy number decreases. This concentration dependence of the excimer dissociation rates illustrates that the state of the monomer (*i.e.*, self-quenched or sequestered) is not a direct consequence of the micelle occupancy number. The exit rate of pyrene from SDS micelles has been determined; it is 4.1×10^{-6} ns^{-1}.[27] Therefore, it is not likely that monomers formed by excimer dissociation diffuse to unoccupied micelles during the lifetime of either monomer. The transfer matrix indicates that excimer dissociates directly to both M_1 and M_2 with no evidence of M_1 conversion to M_2. These observations indicate that pyrene sequestration is not synonymous with singly occupied micelles. In other words, sequestered monomers can be solubilized within micelles which also contain aggregates.

The data in Table 2 also show that, while the rate of monomer self-association k_{M1M2} increases with the pyrene to micelle ratio, the excimer formation rate k_{XM1} is relatively constant with micelle concentration at all but the lowest pyrene to micelle ratio. This result indicates that pyrene excimer formation is not the result of diffusion-controlled collision of excited and ground-state monomers, but occurs after the aggregation of pyrene monomers in SDS micelles. Blackwell et al. also interpreted the constancy of the excimer lifetime as the pyrene concentration was varied in several membranes as an indication that the excimer formation reaction is not diffusion-controlled.[16] The excimer formation rates are close to 2×10^7 M^{-1} s^{-1} which is more than an order of magnitude larger than the rates reported by Blackwell et al. in membranes. However, this value is similar to that of free pyrene observed by Pansu in distearyldimethylammonium bilayers[7] and of pyrene-labeled lipids[18] ob-

TABLE 2: Photokinetic Rates of Pyrene in SDS Micelles[a]

	$-k_{M1*}$[b]	k_{XM1}	k_{M1X}	$-k_{X*}$	k_{M2X}	k_{M1M2}	$-k_{M2*}$
9 mM SDS	15.52 (0.53)[c]	1.82 (0.43)	0.09 (0.13)	2.38 (0.32)	0	1.17 (0.01)	0.65 (0.50)
11 mM SDS	12.94 (0.79)	1.54 (0.90)	2.82 (2.0)	1.92 (0.22)	0.16 (0.23)	0.98 (0.40)	0.10 (0.10)
16 mM SDS	8.69 (3.1)	2.16 (0.37)	2.38 (1.5)	2.14 (0.11)	0.39 (0.55)	0.16 (0.14)	0.26 (0.02)
33 mM SDS	0.96 (0.05)	0.07 (0.03)	0	0.51 (0.20)	0	0	0.37 (0.26)

[a] All rates scaled by 10^{-7}. [b] See text for variable descriptions. [c] Standard deviations in parentheses.

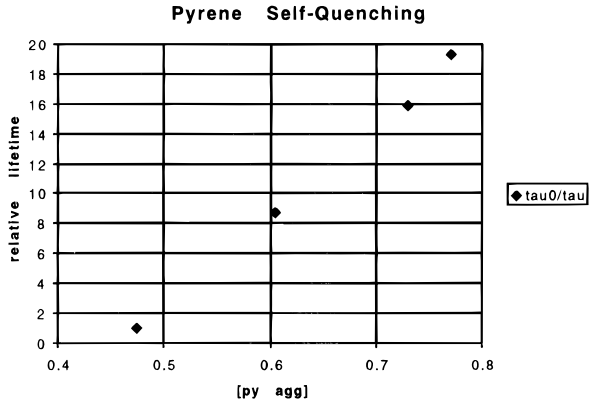

Figure 10. Stern−Volmer plot of the self-quenching of the pyrene aggregate.

served by Sugar. This is not surprising since Blackwell *et al.* calculated the excimer formation rate using the two-state model and used inconsistencies in the concentration dependence of the parameters to illustrate the model limitations.

Although the rate of the excimer formation reaction is not diffusion-controlled, there is a collisional process at the center of the excimer formation mechanism. A Stern−Volmer plot of the self-quenching of the pyrene aggregate is depicted in Figure 10. The slope of the aggregate lifetime ratio is constant with relative aggregate concentration which implies that aggregate self-quenching is a bimolecular process. Of course, without the diffusion controlled bimolecular quenching constant of the aggregate and aggregation number, it is not possible to analyze the influence of diffusion on the aggregate any further. Of course, the implication of this result is that when the aggregate is present, the excimer/monomer ratio is clearly not related to the medium viscosity.

Conclusions

The results presented here indicate that in SDS solutions near the cmc, pyrene molecules exhibit three types of photokinetic behavior. The spectra associated with the decays indicate that there are three types of pyrene monomers in SDS micelles: sequestered monomers in hydrophobic environments that have long intrinsic lifetimes, sequestered monomers in relatively hydrophilic environments that have shorter lifetimes, and self-quenched, aggregated monomers that have extremely short lifetimes and participate in the excimer formation reaction. At high micelle occupancy, pyrene exhibits a fast irreversible excimer formation with significant monomer aggregation. As the micelle occupancy drops, pyrene exhibits a fast reversible excimer formation with significant monomer aggregation. Interestingly, pyrene excimer dissociates into both sequestered and aggregated monomers, but excimer formation is always observed from the aggregate. At very low micelle occupancy, a very slow, apparently irreversible, excimer formation is observed. Neither the spectra nor the decay rates of the excimer forming component show any evidence of aggregate formation at low micelle occupancy, but the spectrum indicates that the excimer forming monomers are in relatively hydrophilic environments.

Acknowledgment. This work was supported by the National Science Foundation (Grants NSF-CHE9314935 and ARI-9313519).

References and Notes

(1) Winnik, M. A.; Dong, D. C. *Can. J. Chem.* **1984**, *62*, 2560−2565.
(2) Kalyanasundaram, K.; Thomas, J. K. *J. Am. Chem. Soc.* **1977**, *99*, 2039−2044.
(3) L'Heureux, G. P.; Fragata, M. *J. Colloid Interface Sci.* **1987**, *117*, 513−522.
(4) Vanderkooi, J. M.; Callis, J. B. *Biochemistry* **1974**, *13*, 4000−4006.
(5) Turro, N. J.; Kuo, P.-L. *Langmuir* **1986**, *2*, 438−442.
(6) Ilharco, L. M.; Santos, A. M.; Silva, M. J.; Martinho, J. M. G. *Langmuir* **1995**, *11*, 2419−2422.
(7) Pansu, R. B.; Yoshihara, K.; Arai, T.; Tokumaru, K. *J. Phys. Chem.* **1993**, *97*, 1125−1133.
(8) Birks, J. B.; Dyson, D. J.; Munro, I. H. *Proc. R. Soc. London, A* **1963**, *275*, 575−588.
(9) Galla, H.-J.; Sackmann, E. *Biochim. Biophys. Acta* **1974**, *339*, 103−115.
(10) Winnik, F. M.; Tamai, N.; Yonezawa, J.; Nashimura, Y.; Yamazaki, I. *J. Phys. Chem.* **1992**, *96*, 1967−1972.
(11) Bertolotti, S. G.; Zimmerman, O. E.; Cosa, J. J.; Previtali, C. M. *J. Lumin.* **1993**, *55*, 105−113.
(12) Warshel, A.; Huler, E. *Chem. Phys.* **1974**, *6*, 463−468.
(13) Sugar, I. P.; Zeng, J.; Vauhkonen, M.; Somerharju, P.; Chong, P. L.-G. *J. Phys. Chem.* **1991**, *95*, 7516−7523.
(14) L'Heureux, G. P.; Fragata, M. *J. Photochem. Photobiol.* **1989**, *3*, 53−63.
(15) Martinho, J. M. G.; Farinha, J. P.; Berberan-Santos, M. N. *J. Chem. Phys.* **1992**, *96*, 8143−8149.
(16) Blackwell, M. F.; Gounaris, K.; Barber, J. *Biochim. Biophys. Acta* **1986**, *858*, 221−234.
(17) Lemmetyinen, H.; Yliperttula, M.; Mikkola, J.; Virtanen, J. A.; Kinnunen, P. K. J. *J. Phys. Chem.* **1989**, *93*, 7170−7175.
(18) Sugar, I. P.; Zeng, J.; Chong, P. L.-G. *J. Phys. Chem.* **1991**, *95*, 7524−7534.
(19) Siemiarczuk, A.; Wagner, B. D.; Ware, W. R. *J. Phys. Chem.* **1990**, *94*, 1661−1666.
(20) Neal, S. L. *J. Phys. Chem.* **1997**, 101.
(21) Sugar, I. P. *J. Phys. Chem.* **1991**, *95*, 7508−7515.
(22) Lofroth, J. E. *J. Phys. Chem.* **1986**, *90*, 1160−1168.
(23) Neal, S. L. *Anal. Chem.* **1997** submitted for publication.
(24) Grieser, F.; Drummond, C. J. *J. Phys. Chem.* **1988**, *92*, 5580−5593.
(25) Siemiarczuk, A.; Ware, W. R. *Chem. Phys. Lett.* **1990**, *167*, 263−268.
(26) Jay, J.; Johnston, L. J.; Scaiano, J. C. *Chem. Phys. Lett.* **1988**, *148*, 517−522.
(27) Almgren, M.; Grieser, F.; Thomas, J. K. *J. Am. Chem. Soc.* **1979**, *101*, 279−291.
(28) Lakowicz, J. R.; Cherek, H.; Balter, A. *J. Biochem. Biophys. Methods* **1981**, *5*, 131−146.
(29) Rossi, T. M.; Warner, I. M. *Anal. Chem.* **1986**, *58*, 810−815.
(30) Shrager, R. I.; Hendley, R. W. *Anal. Chem.* **1982**, *54*, 1147−1152.
(31) Wold, S. *Technometrics* **1978**, *20*, 397−405.
(32) Neal, S. L. *J. Chemom.* **1994**, *8*, 245−261.
(33) Infelta, P. P.; Gratzel, M. *J. Chem. Phys.* **1979**, *70*, 179−186.